C-NCA : Chained Neural Cellular Automata for Fast and Accurate Thermal Ablation Estimation

Jonas Mehtali[1], Juan Manuel Verde[123], and Caroline Essert[1]

[1] ICube, University of Strasbourg, CNRS
[2] IHU Strasbourg - Institute of Image-Guided Surgery
[3] Inria, Strasbourg, France
j.mehtali@unistra.fr

Abstract. Thermal ablation is an increasingly utilized treatment modality for both secondary and primary hepatic tumors. However, it presents significant challenges in treatment planning, particularly when employing multiple applicators. Numerical methods for evaluating the effectiveness of an ablation procedure plan can assist in this task, but they are often computationally intensive or too simplistic, making them impractical for interaction or fast optimization loops in automatic planning. This paper introduces Chained Neural Cellular Automata (C-NCA), a deep learning approach that allows to quickly estimate cell death in thermal ablation procedures. The C-NCA model is trained on a dataset generated by a numerical simulation. When compared to existing methods, the C-NCA achieves comparable accuracy with substantially reduced computation time, thereby making it suitable for interactive planning, instant visualisation, fast automatic planning or even real-time surgical replanning, and potentially enhancing clinical workflows.

Keywords: Simulation · Planning · Thermal ablation · Percutaneous therapy · Deep learning.

1 Introduction

Percutaneous thermal ablation (PTA) is increasingly popular for treating hepatic tumors due to its reduced treatment times and minimal patient trauma [4], and comparable outcomes to surgery for certain indications. However, planning this procedure can be challenging and time-consuming, particularly when multiple applicators are involved, imposing a significant cognitive load on practitioners. This includes sequential use, as observed in RadioFrequency (RF) or MicroWave (MW) Ablation [11], or simultaneous use, as in cryoablation [6]. Numerical methods based on Pennes' bioheat equation [16] have been proposed to estimate ablation areas considering factors such as blood perfusion and the heat sink effect, with calculation times typically ranging in minutes [2,8]. Despite their utility, these numerical methods are not well-suited for optimization loops or interactive planning due to their long computation times.

Approximation methods offer faster estimations but at the cost of precision, particularly when accounting for the heat sink effect. These methods have

demonstrated a Dice coefficient of 0.88 compared to numerical methods [18]. More recently, deep convolutional neural networks, informed by both physics and patient data, have been proposed. They outperform numerical simulations in terms of calculation time, achieving a Dice coefficient of 0.93 for the estimation of thermal propagation with fixed parameters in 0.06 s (16.7 Hz) [12]. A key limitation is the need for retraining when procedural parameters change, such as number of applicators and duration of ablation procedures, hindering the adaptability required for clinical deployment. A robust model capable of rapidly and accurately estimating ablation across varying conditions without retraining would improve procedural planning.

To address this challenge, we propose a physics and patient-informed deep learning method based on Neural Cellular Automata (NCA). NCAs build upon the concept of Cellular Automata (CA) [14] and extend them by integrating neural networks to learn the update rules. They have been successfully applied to reconstruct complex 2D patterns from a seed state, such as dynamic emoji and image reconstruction [13,19]. Recent advancements have extended NCAs to 3D applications, demonstrating their efficiency in multi-dimensional task solving, including generating high-fidelity 3D shapes [22] and regenerating damaged morphologies [10,21]. In our context, NCAs promise to be a powerful tool thanks to their ability to model local interactions among units of space, which is crucial in thermal ablation where the heat distribution and its effects are highly localized. The integration of neural networks enables NCAs to learn complex, non-linear relationships between thermal dosage and tissue response, allowing the model to generalize well to different scenarios and tissue types. Additionally, NCAs can effectively model both spatial and temporal dynamics, which are essential in thermal ablation where the heat distribution changes over time. This adaptive capability, combined with scalability, robustness to variability in initial conditions and environmental factors, and speed, makes NCAs a powerful tool for estimating cell death and model the dynamics in a fast and accurate way.

This paper introduces C-NCA, a new architecture based on chained NCAs, and applies it to thermal-induced tissue death estimation. It incorporates multiple NCA update cycles to estimate heat propagation and vessel heat sink effect, outputting the final cell death estimation using patient-specific spatial tissue properties. Our contributions include:

1. Pioneering the use of Neural Cellular Automata for estimating heat propagation in thermal ablation.
2. Developing the C-NCA approach, which enhances the NCA by replacing operators with multiple NCA updates.
3. Creating a versatile model that supports any number and configuration of applicators, as well as any ablation duration, without the need for retraining.
4. Validating the model on a dataset derived from real-world patients, incorporating comprehensive physical properties.
5. Demonstrating superiority over state-of-the-art in terms of accuracy, robustness, speed, and versatility, making it ideal for interactive planning and optimization.
6. Full dataset available at https://figshare.com/s/a4d1e9a9ededdcdeef39

2 Methods

2.1 General architecture

We introduce a novel approach, named *Chained Neural Cellular Automata* (or C-NCA) that diverges from conventional NCA pipelines [13,19,21] by eliminating Sobel filtering, stochastic updates, and life masking. Sobel filtering and life masking were eliminated, as these tasks can be learned by the model using the chained NCA update steps. Stochastic updates were removed due to a lack of evidence of their benefit [3]. This elegant simplification makes C-NCA computationally more efficient while retaining the same expressiveness.

The proposed C-NCA pipeline is summarized in Fig.1. It receives as input a voxel grid of any arbitrary size, that constitutes the initial state ②. Each voxel of the grid ① comprises five distinct channels representing tissue survivability, ablation duration encoded into the voxels of the applicator, perfusion rate, density ρ, and specific heat capacity c. To mitigate numerical discrepancies, each range of values was normalized to the interval [0, 1] through min-max scaling $x' = (x - min(x))/(max(x) - min(x))$, where the maximal and minimal values are based on theoretical limits for each channel.

The pipeline operates iteratively, where an initial seed state is progressively refined in an NCA upade process ③ that consists of N_C iterations of N_S chained NCA update steps ④. Each NCA update step ⑤ consists of a neural network composed of two 3D convolutional layers, with a ReLU activation in between. Both convolutional layers employ $3 \times 3 \times 3$ kernels with a padding of 1. The first convolution expands the feature representation by a factor of three, while the second convolution compresses these back to the original five-channel format, ensuring continuity in feature propagation.

In each NCA update step, the neural network takes the previous state as input and adds it into the output ⑥ to generate the next state. This iterative process allows the solution to "grow" with each iteration, gradually refining the predicted thermal damage. Each update passes its output as input to the subsequent NCA update step, facilitating a structured and hierarchical refinement

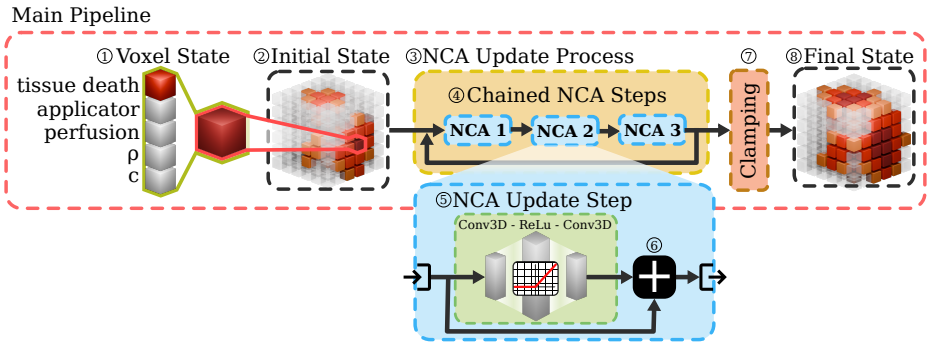

Fig. 1: General architecture of the main C-NCA pipeline

of predictions. The optimal number of iterations N_C is discussed in Section 3.3. Upon completion of the NCA update process, the first channel representing tissue death is clamped ⑦ to the [0, 1] interval to enforce the theoretical range in the final state ⑧.

2.2 Synthetic dataset generation

To train our model, we generated a dataset using conventional numerical simulations to teach our model thermal propagation and tissue response during ablation procedures. The numerical simulations were based on the Pennes bioheat equation [16] to solve the following diffusion equation:

$$\rho_{mat} c_{mat} \frac{\Delta T}{\Delta t} = \nabla(d\nabla T) + Q_{bio} + Q_{ext} \tag{1}$$

with T as the temperature, Δt the timestep set to 0.025 seconds to satisfy a stability criterion detailed in [8], $\nabla(d\nabla T)$ the heterogeneous heat conduction term, Q_{bio} the biological heat source, and Q_{ext} the external heat source. Terms ρ_{mat} and c_{mat} are the material's density and specific heat capacity. The biological heat $Q_{bio} = \omega_b \rho_b c_b (T_b - T) + Q_{met}$ includes ω_b the blood perfusion rate, ρ_b blood density, c_b blood specific heat capacity, T_b local and average blood temperature, and Q_{met} metabolic heat production. The equation models heat exchange in tissue due to blood perfusion and metabolism. In organs like the liver, blood vessels act as a heat sink, affecting ablation.

To quantify heat deposition resulting from energy transfer by external sources, we used Equation 2 found in Hall et al. [9], which models RF or MW ablation:

$$Q_{ext} = \frac{1}{2} \sigma_{mat} \sum_{i=1}^{I} |\nabla V_i|^2 \tag{2}$$

where V_i is the electrical potential of antenna i out of I antennas, and σ_{mat} is electrical conductivity. For the computation of V_i, readers are referred to the work by A. M. Qadri [17]. All physical properties were sourced from *IT'IS Database for Thermal and Electromagnetic Parameters of Biological Tissues* [1].

The heat propagation simulation is paired with a three-state cell death model proposed by O'Neill *et al.* [15] to assess tissue states (alive, damaged, or dead). In this model, cell death is computed based on the thermal dose received by the tissue, which is a function of both temperature and exposure time. The approach defines thresholds for transitioning between the alive, damaged, and dead states. Damage accumulated by cells over time, as they are exposed to elevated temperatures, is then used to determine the final state of the tissue.

A GPU-based Finite Difference (FD) method inspired by [8] was used for computational efficiency. It discretizes space into isotropic voxels where heat transfer is calculated for thermal conductivity in the x, y, and z directions. To determine the regions of interest (ROI) for the simulations, bounding boxes are created for each applicator's emission zone and expanded by a 50 mm margin in every direction [5].

3 Experimental validation

3.1 Dataset

A dataset of 3500 synthetic multi-channel and multi-resolution patient volumes with antennas was generated. The dataset includes 25 tumors in 7 anatomies extracted from the 3D-IRCADb-01 database [20], which contains 3D CT scans of patients with hepatic tumors, as well as segmentations of the anatomical structures. Among the 25 tumors, 12 were natively present in the 7 chosen anatomies. The 13 additional tumors were extracted from other patients and slightly modified (scaled, rotated, translated), then added near vessels at an average distance of 3.6±0.6 mm, to assess the heat sink effect on ablation volumes. Average tumor volume was 1421±145 mm^3, reflecting typical tumors treated using thermal ablation [7]. Each combination of patient/tumor was treated as a separate case.

For training, we used 20 cases in 5 anatomies and ran 125 simulations per case. For each simulation, an equiprobable allocation of 1 to 3 non-overlapping applicators of identical geometry was generated, randomly placed at a maximum distance of 40 mm from a tumor, respecting a minimal distance of 10 mm between applicator tips, and randomly oriented within the patient's liver to encompass all possible configurations of applicator placements, for a total of 2500 generated volumes. Similarly, for testing, we used the same 20 cases and ran 25 simulations per case with 1-5 generated applicators, for a total of 500 volumes. For validation, we used the 5 remaining cases in the 2 anatomies unseen during training/testing, ran 100 simulations per case with 1-5 generated applicators, for a total of 500 volumes. Testing and validation have been performed using more applicators than training, to evaluate the ability of C-NCA to extrapolate multi-applicator ablations with a higher needle count.

Numerical simulations of thermal propagation and cell states were computed using a state-of-the-art finite difference method (FDM) and a validated cell death model. Synchronous ablations of 300 seconds were applied per applicator. The resulting volumes were subsequently downsampled from an initial isotropic voxel discretization of 2 mm to 3 mm and 4 mm resolutions.

Our simulations used the segmented organs from the database (liver, arteries and veins, tumors), as masks with different tissue properties (density, heat capacity, thermal and electrical conductivity) in the initial state.

3.2 Training and Evaluation

During the training phase, 2500 instances from the dataset depicted in Section 3.1 were utilized. The tissue death channel was established as the target, while the other channels were used to construct the seed state. The generated seed, with cell death channel set to zeros, was used as the input. A further 500 additional instances were reserved for validation and early stopping protocols.

Data Augmentation. In this study, 90° increment volume rotation and axial flipping were implemented as the main data augmentation modalities.

Data Reinjection. Substituting 12.5% of the current batch with output states from a previous batch that exhibited the highest loss, thereby enabling continued estimation, facilitated further training without excessive memory allocation for gradient computation. This approach has shown to enhance model robustness and prevent divergence across iterations, while additionally concentrating training efforts on more challenging cases [13].
Loss Function. A modified mean squared error (MSE) loss was used to reduce the penalization of tissue death predictions exceeding 100% or falling below 0%, as these values are clamped in the pipeline. Strong penalization of these out-of-bounds values would impede learning without affecting final predictions. A scaling factor of 0.1 was applied to out-of-range predictions, allowing the model to explore boundary conditions without disproportionate punishment. This loss function was applied before final clamping and only to the first channel, leaving other channels to the model's discretion.
Solution Convergence and Persistence. In order to facilitate the convergence of the model towards a solution and ensure its stability in subsequent iterations, the model was trained across a spectrum of random iteration counts for the chained NCA steps, ranging from 7 to 75. This methodological approach guarantees the model's adaptability by preventing specific training towards any predetermined set of update cycle iterations, thereby enhancing its generalizability [13]. This strategy proved particularly beneficial in identifying the optimal range of update iterations as discussed in Section 3.3.
Training Completion. In order to estimate the completion of training and facilitate efficient early stopping, the mean loss between consecutive epochs was evaluated. Detection of a plateau or an increment in the mean loss would initiate the termination of the training process.

We trained three networks specialized in 2 mm, 3 mm and 4 mm resolutions without architecture change across 2500 volumes as detailed in Section 3.1. Power was set to 50 W to simulate RF, with each case involving 1 to 5 sequential ablations. Within the same volume, each applicator was active for 300 s, for total simulation times ranging from 300 s to 1500 s of asynchronous heating. The metrics assessed included the total computation time required to generate results and the deduced frames per second (fps) to evaluate the responsiveness of result generation, and the root-mean-square error (RMSE) between the synthetic truth at a resolution of 2 mm (reference) and the model's output, which was utilized to evaluate each model's fidelity to the synthetic truth.

3.3 Results and Analysis

The training and evaluation were performed on a Core-i9 desktop computer with 32.0 GiB RAM and a GeForce RTX™ 4080 SUPER with 10,240 CUDA cores.

Table 1 summarizes the obtained results. It can be observed that the C-NCA method was able to accurately reproduce the RFA simulations, with low average RMSE, ranging from 1.43% for the 2mm resolution to 1.74% for the 4 mm resolution (Fig.2b). Visually, the results look very similar, as illustrated on Fig.3, which is consistent with the numerical results.

Table 1: Benchmark results of FDM and C-NCA on the test set

Method	Resolution	Avg. time	(STD)	fps	Avg. RMSE	(STD)
-	mm	s	s	Hz	%	%
FDM	2	0.10	0.0514	10	-	-
	3	0.04	0.0174	25	1.63%	0.38%
	4	0.03	0.0101	33	1.88%	0.43%
C-NCA	2	0.0037	0.0014	270	1.43%	0.76%
	3	0.0029	0.0011	345	1.79%	0.97%
	4	0.0021	0.0009	476	1.74%	0.77%

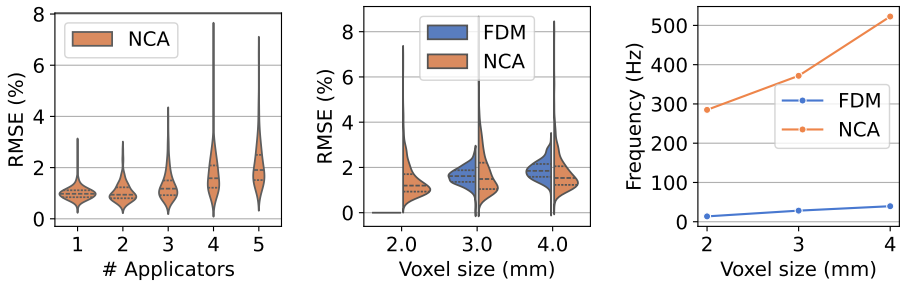

(a) RMSE per # of applic. (b) RMSE per voxel size (c) Frequency per voxel size

Fig. 2: (a) RMSE (%) depending on number of applicators for a resolution of 4 mm; (b) RMSE (%) and (c) frequency (fps) depending on voxel resolution (mm)

The computation times were significantly lower using C-NCA than FDM (see Fig.2c). The fastest approach in the literature [12] could simulate 7 min of heating from a single applicator in 0.06 seconds at a resolution of 4 mm (≈16 fps), while our approach reaches 0.0021 seconds (476 fps) for the same resolution with up to 5 applicators and a total of 25 min. The highest resolution of 2 mm provides an average frame rate exceeding 250 fps, ensuring smooth interaction with seamless visual updates. Training a model at an even higher 1 mm resolution would require more computational power than what was available for this study.

We experimented three variants of the update process, respectively with a number $N_S \in \{1, 2, 3\}$ of NCA update steps. N_C was adjusted so that $N_C \times N_S$ stays constant, to enable fair comparison of performance under equal computational budgets, leaving broader architectural exploration for future work.

The findings indicate that the model with three chained NCA update steps surpassed the performance of the others with a resulting RMSE value of 1.74% on the test dataset, against 9.16% for the one-step, and 2.02% for the two-steps model (results for the 4mm trained models). Further research would be needed to assess whether increasing the number of chained NCA updates could yield any additional improvements in performance.

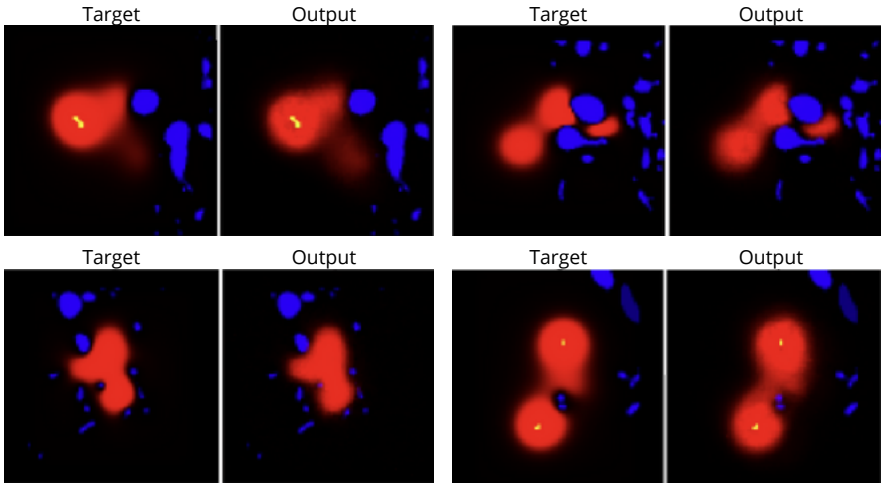

Fig. 3: 2D slices of target (FDM, 2mm) and output (C-NCA, 2mm) on 4 different tumors: tissue death (red), vessels (blue) and ablation applicator (yellow)

To identify the optimal number of iterations N_C, the C-NCA model was executed on the test dataset with 100 iterations and the result after each update cycle was extracted for evaluation. Evaluation of the minimum RMSE across outputs revealed that the optimal number of iterations varied with spatial resolution: 27 iterations for 2 mm, 20 for 3 mm, and 13 iterations for 4 mm. These optimized iteration counts were subsequently employed throughout all experiments to ensure consistent and effective performance.

The model's adaptability to multi-applicator ablation was assessed through the RMSE score for the 2 mm C-NCA with 1 to 5 applicators. The results indicated a consistent RMSE score across different numbers of applicators (Fig. 2a), demonstrating that this architecture can accurately predict outcomes for multi-ablation and multi-duration procedures, maintaining consistent quality even with more applicators than it was trained on. Moreover, we observed that perfusion layers with high blood flow grow outwards, nicely capturing heat sink effects.

4 Conclusion and Future Work

We introduced an approach to estimate the heat induced tissue death in PTA based on a chained NCA architecture. While not directly producing a heat map, it accurately estimates cell death induced by thermal damage by implicitly modeling temperature field effects and evolution, going beyond heat distribution, with low RMSE and high speed. The model is computationally efficient, characterized by a mere 12,210 learned parameters, and is capable of operating on a standard desktop computer due to its implementation through basic 3D convolutions. It can compute 25 minutes of treatment at a frequency up to 476 fps, making it suitable for interactive simulations and optimization loops.

While our current model assumes a static environment, the C-NCA architecture has the capacity to model dynamic settings, such as model temperature-dependent tissue properties and fluid dynamics, with appropriate training data. The method has been tested with RF ablation parameters but could also be adapted to other thermal ablation modalities. Future research could include training a generic C-NCA model to dynamically estimate ablation-induced tissue death at various energy levels and applicator models by adding channels to encode these parameters. This research is intended for integration into interactive planning software and automated planning tools. Though based on synthetic data, our evaluation uses a robust pipeline with state-of-the-art FDM and a validated cell death model, providing a solid foundation for clinical translation. Finally, although C-NCA have been conceived with our context and application in mind, we believe it is generic enough to be used in many other fields.

Acknowledgments. This work of the Interdisciplinary Thematic Institute HealthTech, as part of the ITI 2021-2028 program of the University of Strasbourg, CNRS and Inserm, was supported by IdEx Unistra (ANR-10-IDEX-0002) and SFRI (STRAT'US project, ANR-20-SFRI-0012) under the framework of the French Investments for the Future Program. It has been partially funded under the framework of the French Investments for the Future Program, by French state funds managed within the "Plan Investissements d'Avenir", by the ANR (reference ANR-10-IAHU-02).

Disclosure of Interests. The authors have no conflict of interest to declare.

References

1. IT'IS Database for thermal and electromagnetic parameters of biological tissues, Version 4.2. null . https://doi.org/10.13099/vip21000-04-2
2. Audigier, C., Mansi, T., Delingette, H., Rapaka, S., Mihalef, V., Carnegie, D., Boctor, E., Choti, M., Kamen, A., Ayache, N., Comaniciu, D.: Efficient Lattice Boltzmann Solver for Patient-Specific Radiofrequency Ablation of Hepatic Tumors. IEEE Transactions on Medical Imaging **34**(7), 1576–1589 (2015). https://doi.org/10.1109/tmi.2015.2406575
3. Catrina, S., Catrina, M., Băicoianu, A., Plajer, I.C.: Learning About Growing Neural Cellular Automata. IEEE Access **12**, 45740–45751 (2024). https://doi.org/10.1109/access.2024.3382541
4. Chen, M.S., Li, J.Q., Zheng, Y., Guo, R.P., Liang, H.H., Zhang, Y.Q., Lin, X.J., Lau, W.Y.: A Prospective Randomized Trial Comparing Percutaneous Local Ablative Therapy and Partial Hepatectomy for Small Hepatocellular Carcinoma. Annals of Surgery **243**(3), 321–328 (2006). https://doi.org/10.1097/01.sla.0000201480.65519.b8
5. Crocetti, L., de Baére, T., Pereira, P.L., Tarantino, F.P.: CIRSE Standards of Practice on Thermal Ablation of Liver Tumours. CardioVascular and Interventional Radiology **43**(7), 951–962 (2020). https://doi.org/10.1007/s00270-020-02471-z
6. Dodi, R., Ferraguti, F., Ristolainen, A., Secchi, C., Sanna, A.: Planning and Simulation of Percutaneous Cryoablation. AASRI Procedia **6**, 118–122 (2014). https://doi.org/10.1016/j.aasri.2014.05.017

7. Galle, P.R., Forner, A., Llovet, J.M., Mazzaferro, V., Piscaglia, F., Raoul, J.L., Schirmacher, P., Vilgrain, V.: EASL Clinical Practice Guidelines: Management of hepatocellular carcinoma. Journal of Hepatology **69**(1), 182–236 (2018). https://doi.org/10.1016/j.jhep.2018.03.019
8. Golkar, E., Rao, P.P., Joskowicz, L., Gangi, A., Essert, C.: GPU-based 3D iceball modeling for fast cryoablation simulation and planning. International Journal of Computer Assisted Radiology and Surgery **14**(9), 1577–1588 (2019). https://doi.org/10.1007/s11548-019-02051-8
9. Hall, S.K., Ooi, E.H., Payne, S.J.: A Mathematical Framework for Minimally Invasive Tumor Ablation Therapies. Critical Reviews in Biomedical Engineering **42**(5), 383–417 (2014). https://doi.org/10.1615/critrevbiomedeng.2014011825
10. Horibe, K., Walker, K., Risi, S.: Regenerating Soft Robots Through Neural Cellular Automata. In: Hu, T., Lourenço, N., Medvet, E. (eds.) Genetic Programming. pp. 36–50. Springer International Publishing, Cham (2021). https://doi.org/10.1007/978-3-030-72812-0_3
11. Livraghi, T., Goldberg, S.N., Lazzaroni, S., Meloni, F., Ierace, T., Solbiati, L., Gazelle, G.S.: Hepatocellular Carcinoma: Radio-frequency Ablation of Medium and Large Lesions. Radiology **214**(3), 761–768 (2000). https://doi.org/10.1148/radiology.214.3.r00mr02761
12. Meister, F., Audigier, C., Passerini, T., Lluch, È., Mihalef, V., Maier, A., Mansi, T.: Fast Automatic Liver Tumor Radiofrequency Ablation Planning via Learned Physics Model. Lecture Notes in Computer Science pp. 167–176 (2022). https://doi.org/10.1007/978-3-031-16449-1_17
13. Mordvintsev, A., Randazzo, E., Niklasson, E., Levin, M.: Growing Neural Cellular Automata. Distill **5**(2) (2020). https://doi.org/10.23915/distill.00023
14. Neumann, J.V.: Theory of Self-Reproducing Automata. University of Illinois Press, Champaign, IL, USA (1966)
15. O'Neill, D.P., Peng, T., Stiegler, P., Mayrhauser, U., Koestenbauer, S., Tscheliessnigg, K., Payne, S.J.: A Three-State Mathematical Model of Hyperthermic Cell Death. Annals of Biomedical Engineering **39**(1), 570–579 (2010). https://doi.org/10.1007/s10439-010-0177-1
16. Pennes, H.H.: *Analysis of Tissue and Arterial Blood Temperatures in the Resting Human Forearm*. Journal of Applied Physiology **1**(2), 93–122 (1948). https://doi.org/10.1152/jappl.1948.1.2.93
17. Qadri, A.M., Chia, N.J., Ooi, E.H.: Effects of saline volume on lesion formation during saline-infused radiofrequency ablation. Applied Mathematical Modelling **43**, 360–371 (Mar 2017). https://doi.org/10.1016/j.apm.2016.11.032, http://dx.doi.org/10.1016/j.apm.2016.11.032
18. Rieder, C., Kroeger, T., Schumann, C., Hahn, H.K.: GPU-based Real-Time Approximation of the Ablation Zone for Radiofrequency Ablation. IEEE Transactions on Visualization and Computer Graphics **17**(12), 1812–1821 (2011). https://doi.org/10.1109/TVCG.2011.207
19. Ruiz, A.H., Vilalta, A., Moreno-Noguer, F.: Neural Cellular Automata Manifold. 2021 IEEE/CVF Conference on Computer Vision and Pattern Recognition (CVPR) pp. 10015–10023 (2021). https://doi.org/10.1109/cvpr46437.2021.00989
20. Soler, L., Hostettler, A., Agnus, V., Charnoz, A., Fasquel, J.B., Moreau, J., Osswald, A.B., Bouhadjar, M., Marescaux, J.: 3D Image Reconstruction for Comparison of Algorithm Database: A patient specific anatomical and medical image database. Tech. rep., IRCAD Strasbourg, France (2010)

21. Sudhakaran, S., Grbic, D., Li, S., Katona, A., Najarro, E., Glanois, C., Risi, S.: Growing 3D Artefacts and Functional Machines with Neural Cellular Automata. In: ALIFE 2021: The 2021 Conference on Artificial Life. MIT Press (2021). https://doi.org/10.1162/isal_a_00451
22. Zhang, D., Choi, C., Kim, J., Kim, Y.M.: Learning to Generate 3D Shapes with Generative Cellular Automata (2021). https://doi.org/10.48550/arXiv.2103.04130